Radiative lifetimes and linewidth broadening of single InAs quantum dots in an $Al_xGa_{(1-x)}As$ matrix

Radiative lifetimes and linewidth broadening of single InAs quantum dots in an $Al_xGa_{(1-x)}As$ matrix

S. C. M. Grijseels[a,*], J. van Bree[a], P. M. Koenraad[a], A. A. Toropov[b], G. V. Klimko[b], S. V. Ivanov[b], C. E. Pryor[c], A. Yu. Silov[a]

E-mail: * s.c.m.grijseels@tue.nl
[a] Photonics and Semiconductor Physics Group, COBRA Research Institute, Eindhoven University of Technology, 5600 MB Eindhoven, The Netherlands
[b] Centre of Nanoheterostructure Physics, Ioffe Institute, 194021 St. Petersburg, Russian Federation
[c] Department of Physics and Astronomy and Optical Science and Technology Center, University of Iowa, Iowa City, IA 52242, USA

Abstract. We investigate the linewidths and radiative lifetimes of single InAs quantum dots embedded in the ternary matrix $Al_xGa_{(1-x)}As$ as function of aluminum composition. For an increasing aluminum content, we find that the average of the measured linewidths of individual transitions increases. Furthermore, we find that the distribution of the measured linewidths broadens. We infer that the linewidth broadening is the result of spectral wandering caused by inhomogeneities and local defects in the surrounding $Al_xGa_{(1-x)}As$ matrix. Local charging and de-charging of defects polarize quantum dots in their vicinity thereby shifting the energy states of the exciton transition in time through the quantum confined Stark effect. The intrinsic radiative lifetimes of numerous quantum dots were determined. We suggest that the observed variation in radiative lifetime at a given photon energy is explained by the influence of an in-plane electric field on the oscillator strength of the electron–hole pair.

1. Introduction

After almost half a century one could contemplate if the GaAs based semiconductor industry would have ever been so successful without the application of its ternary counterpart $Al_xGa_{(1-x)}As$ [1, 2]. Since the late sixties it was long recognized that combining the two lattice–matched materials, each owing its unique properties, would offer a huge variety in optoelectronic devices and applications [3, 4, 5, 6, 7, 8, 9, 10, 11]. For instance, the well-established technique of modulation doping can be utilized to achieve ultrahigh mobilities in electronic devices [2, 3]. On the other hand, exploiting the fact that the free exciton transition energy strongly depends on the Al concentration opens up the possibility to tune the confinement of both electrons and holes, which in turn allows for device operation up to room temperature [4, 5, 6].

In this report, we draw our attention to the application of the $Al_xGa_{(1-x)}As$ as a matrix element in combination with zero dimensional components, i.e., InAs quantum dots (QDs). The optical properties of InGaAs quantum dots inside the GaAs matrix have been studied extensively for their potential role in quantum application devices [12, 13, 14, 15]. The motivation for these experiments can be found in the fact that for quantum operations the coherence time of any two-level system, in this case the exciton transition inside the quantum dot, is of utmost importance. This constrains the homogeneous linewidth Γ of the transition to be preferably at or close to the transform-limited optical transition, at which point the linewidth is solely determined by the radiative lifetime τ_X of the emitter itself [16, 17, 18, 19]. On timescales much shorter than 100 ps, various scattering processes, such as electron-electron scattering and phonon scattering, cause homogeneous broadening of the transition [20, 21, 22]. On timescales much larger than the intrinsic radiative lifetime, the optical transition energy is dynamically broadened as a result of the quantum confined Stark effect (QCSE), which shifts the states of the transition in time (the so-called spectral diffusion or spectral wandering) [17, 23].

In view of the numerous experiments conducted on the InAs/GaAs quantum dot system and its various device applications, one would expect that a sizable amount of literature would be available for the InAs/AlGaAs system. Potentially, the system comprising InAs quantum dots embedded in an $Al_xGa_{(1-x)}As$ matrix could solve some of the ongoing issues of the InAs/GaAs quantum dot system. Most importantly, as previously mentioned, the incorporation of aluminum into the GaAs matrix leads to the achievement of room temperature operation of the system [24]. Moreover, the deep confinement of charged carriers could lead to very low decoherence rates, which are important for applications of quantum computers built up out of III–V semiconductor materials. Surprisingly however, up until now, not a single paper has been published that addresses the radiative properties of single InAs quantum dots inside the $Al_xGa_{(1-x)}As$ matrix.

We investigate the spectral linewidth of individual InAs quantum dots embedded in $Al_xGa_{(1-x)}As$ for three different samples of varying aluminum composition ($x = 0.13$, 0.23 and 0.33) using low temperature micro-photoluminescence (μPL) spectroscopy. We probe the inhomogeneous broadening of the exciton ground state transition for energies above 1.1 eV, a limit set by the Si based detectors. The radiative lifetime of the exciton ground state emission was determined by time-resolved μPL spectroscopy (TRPL). Different excitation wavelengths were used to excite both above and below the absorption band edge of the samples.

2. Experimental details

The samples were grown by molecular beam epitaxy using a GaAs semi-insulating (undoped) substrate. For the 13% and 23% Al samples, an $Al_xGa_{(1-x)}As$ barrier layer of approximately 200 nm was grown on top of a 300 nm GaAs buffer layer. After barrier layer growth, 1.8–1.9 mono layers (ML) of InAs were deposited as a seeding layer for the quantum dot formation. Finally, the samples were capped with 100 nm of $Al_xGa_{(1-x)}As$ followed by 2 ML of GaAs to prevent oxidation of the $Al_xGa_{(1-x)}As$ layers. For the 33% Al sample, 200 nm $Al_{0.33}Ga_{0.67}As$ was grown on top of a 20 nm thick AlAs buffer layer. After the quantum dot formation, the sample was capped with 55 nm of $Al_{0.33}Ga_{0.67}As$ followed by quantum dot overgrowth to allow for determination of the dot density and size distribution by atomic force microscopy. The aluminum concentration of all three samples was determined using reflectivity measurements at 70 K [25, 26].

In order to optically resolve single quantum dots,

we use Au masking containing apertures of variable size (33% Al sample) or we make freestanding mesas (23% and 13% Al samples) of 150 nm in height. Using standard lithography, both apertures and mesas were created with an average lateral size of 1 μm^2. The creation of the mesas involved etching of the sample and the creation of sidewalls close to the nanocrystal structures. The masking was done on top of the sample surface, leaving the sample structure unharmed. A pitch size of 3 μm was used to allow for the Ti:Sapphire laser, having a spot size of $\sim$1 μm in diameter, to address the apertures (mesas) individually. Prior to the creation of the mesas, we check the linewidth of several isolated dots in the 13% and 23% samples. From these measurements, we exclude any radiative broadening effects of the sidewalls of the mesas.

For the TRPL measurements, the Ti:Sapphire laser was operating at 76 MHz with a pulse width of 5 ps. μPL measurements were performed with continuous wave operation in backscattering geometry using a 100$\times$ objective. After collection, the photoluminescence signal was dispersed in a 0.5 m spectrometer and either registered on a Si charge coupled device (CCD) or on a Si avalanche photo diode (APD). Using a HeNe calibration light source, the spectral resolution of the setup was determined and found to vary from 50 μeV at 1.18 eV to 100 μeV at 1.62 eV. The full widths at half maximum of individual transitions were determined by using either a Gaussian or a Lorentzian fitting function, or a combination of the two, i.e., a Voigt function. Recording a histogram of the reflected laser light from the sample surface, the instrumental response function (IRF) was found to be 650 ps. However, least squares deconvolution of the data fixes the resolution to the size of the bin width of the time correlator card, which is 37 ps.

3. Experimental results

3.1. Linewidth broadening

Fig. 1 shows the macro photoluminescence spectra and the measured linewidth of individual dots as a function of photon energy for the three samples. The macro photoluminescence spectra are normalized over the entire ensemble and the energy shift in maximum photoluminescence intensity reflects both the increased height of the confinement barrier as a result of the change in $Al_xGa_{(1-x)}As$ band gap energy, as well as the somewhat reduced dimension of the quantum dot size for increasing aluminum content [27]. The enhancement of the confinement barrier height was confirmed from temperature dependent measurements, which at room temperature revealed strong photoluminescence intensities for the sample having the highest aluminum content.

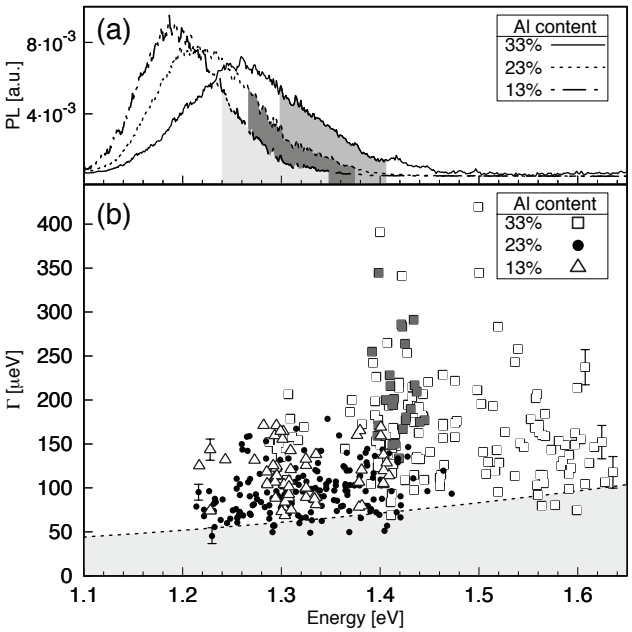

Figure 1. (a) Macro photoluminescence spectra of the three samples at 10 Kelvin, using an InGaAs CCD camera in combination with a 20$\times$ objective and 0.3 m spectrometer. All spectra were excited using a continuous wave laser diode operating at 1922 meV with 200 μW power density. (b) Optical linewidth Γ as function of photon energy for varying aluminum composition measured on the Si CCD camera for below $Al_xGa_{(1-x)}As$ band gap excitation energies. The gray area underneath the horizontal dashed line indicates the detection limit of the setup as function of energy. The error bars for the selected dots at the low and high energy side of the spectrum reflect the error in the measured full width at half maximum. All the measurements were done at 4.2 K.

For the linewidth measurements, we used below $Al_xGa_{(1-x)}As$ band gap energies to optically excite the dots, i.e., 1589 meV for the 13% and 23% Al samples and 1771 meV for the 33% Al sample (filled squares). The latter also was excited with an excitation energy of 1922 meV (open squares) quasi-resonant with the $Al_{0.33}Ga_{0.67}As$ band gap energy of 1940 meV [25, 28]. The collection time for each individual point was 10 s for the 13% Al sample and 30 s for the 23% and 33% Al samples. To rule out the possibility of multi exciton emission, the power dependency of the photoluminescence intensity of each single line was carefully checked and only those that showed linear dependency were included in the linewidth measurements [29].

To study the dependency of the linewidths on the aluminum concentration, we use the macro photoluminescence spectra of Fig. 1a to identify an ensemble of dots within each of the three samples that are equally comparable in terms of photoluminescence intensity and are still considered to be part of the main photoluminescence peak. For each of the ensembles, we calculate the cumulative histograms of all the

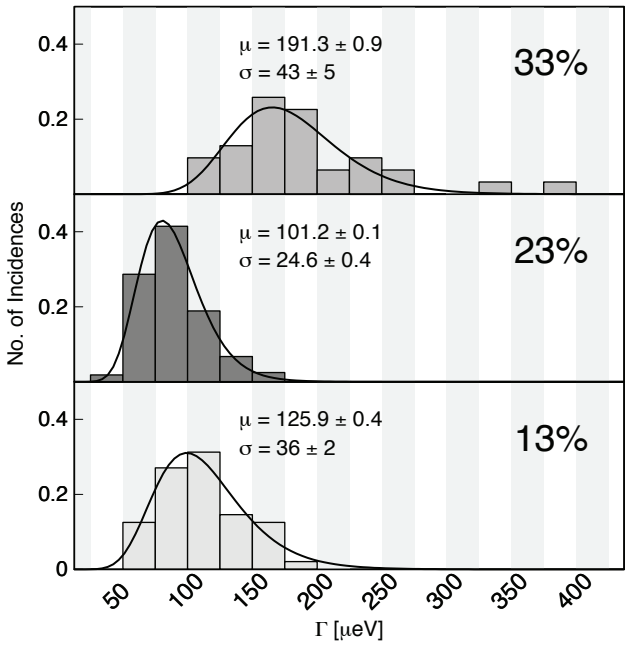

Figure 2. Cumulative histograms of the measured linewidths of the three samples, normalized to the total number of incidences, for the energy ranges as indicated in Fig. 1a, using a bin width of 25 μeV. The figure also shows the computed values (in μeV) for the mean μ and standard deviation σ using a log-normal distribution function as a fit (solid black line).

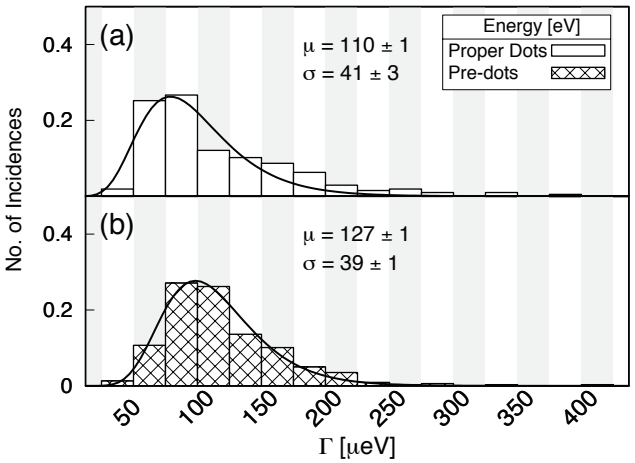

Figure 3. Histograms showing the distribution of the measured linewidths, which were obtained by combining the results from all three samples, for all excitation energies used. The histograms are normalized to the total number of incidences, using two different classes of dots, i.e., the *proper dots* (a) and the *pre-dots* (b). The distinction between the two classes is based on a difference in quantum dot size, as is determined from the macro photoluminescence spectra of Fig. 1a. The used bin width is 25 μeV. The figure also shows the computed values (in μeV) for the mean μ and standard deviation σ using a log-normal distribution function as a fit (solid black line).

linewidths for all excitation energies within an energy range of 110 meV using a bin width of 25 μeV and a lognormal distribution function as a fit. The results of these calculations together with the fitting function (black solid lines) are shown in Fig. 2. Also shown are the computed values (in μeV) of the mean average μ and its standard deviation σ. From the histograms, it is clear that the average linewidths for the 33% Al sample are increased in comparison to those of the two other samples, which are comparable within the resolution limit of our setup. Moreover, the distribution of the linewidths of the 33% Al sample is more dispersed.

The dependence of the linewidth on quantum confinement is investigated. We fit each of the three macro photoluminescence spectra of Fig. 1a with a single lognormal distribution function. From the fits, we obtain the standard deviation σ_x of the ensemble photoluminescence spectra for every aluminum composition x. We distinguish between quantum dots, which we consider to be part of the main photoluminescence envelope function, and dots that are located at the high energy side of photoluminescence spectra, with a photon energy larger than $2 \times \sigma_x$ compared to the peak photoluminescence energy position. In the following, we will refer to the first class of dots as *proper dots*. Quantum dots with a ground state exciton transition in the high energy tail of the photoluminescence distribution are dubbed *pre-dots*, because we think that these dots are smaller than the proper dots.

Fig. 3 shows the cumulative linewidth distribution of the three samples as function of Γ based on this classification. Using the histograms of Fig. 3, we determine the mean average value of the full width at half maximum and its standard deviation for both ensembles. For the proper dots, the measured average Γ is (110 $\pm$ 41) μeV and for the pre-dots the average Γ is (127 $\pm$ 39) μeV. We conclude that the proper dots have an average Γ, which is slightly smaller than those of the pre-dots, with a comparable distribution.

3.2. Radiative lifetimes

As pointed out previously, spectral wandering is a process that depends on the dynamics of a fluctuating environment. Here we would like to address the influence of the electrostatic environment of the dot. This means that we are interested in radiative processes, which occur on a timescale faster than the spectral diffusion time [30]. We perform TRPL measurements to study the nature of the ground state exciton transition. Fig. 4a shows the radiative lifetimes as function of photon energy for the three samples. The photon energy range for our time-resolved measurements was chosen such that it covers a comparable amount of both proper dots and pre-dots. An example of a lifetime transient together with the IRF recorded on the APD is shown in

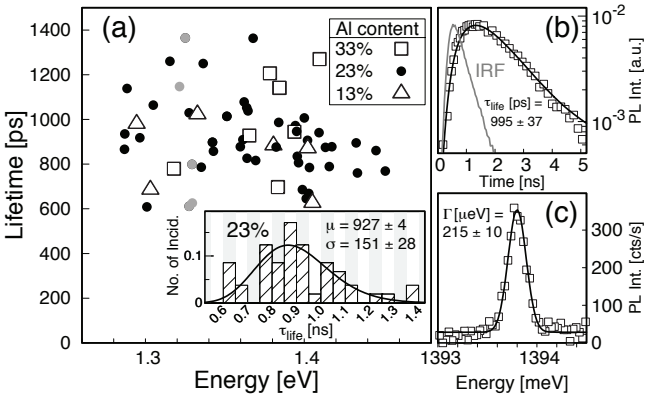

Figure 4. (a) Radiative lifetime as function of ground state photon energy for varying aluminum composition measured on the avalanche photodiode (APD) for below $Al_xGa_{(1-x)}As$ band gap excitation energies. The size of the filled circles for the 23% Al sample indicate the magnitude of the measurement error in the lifetime of $\sim$40 ps. A selection of dots of comparable photon energy (1326 ± 5) meV in the 23% sample, which were all excited with the same excitation energy (1718 meV) and an equivalent power density of 4 Wcm^{-2}, is indicated by the light gray dots. The inset shows the histogram of the measured lifetimes of the 23% Al sample and the corresponding values (in picoseconds) using a bin width of 50 ps. (b) Typical lifetime transient for a quantum dot at 1393.8 meV in the 33% Al sample. The solid black line is a fit to the measured data. Also indicated in the figure are the radiative lifetime of the dot and the instrument response function (IRF) (gray solid line). (c) Spectrum for the same dot as in (b) measured with the APD. A Gaussian fit (solid line) was used to determine the full width at half maximum of 215 μeV. The background counts of the spectrum stem from the detector's dark count rate of $\sim$40 Hz. All the measurements were done at 4.2 K.

Fig. 4b. Fig. 4c shows the corresponding spectrum of the dot. We only excited the dots non-resonantly, with excitation energies below and above the wetting layer emission energy [31]. Also here, we only include the radiative lifetime values from exciton transitions that show a linear dependency of the photoluminescence intensity on the excitation density. For the 13% and 33% Al samples, we have employed excitation energies of 1589 and 1768 meV, respectively. The 23% Al sample was excited at 1718, 1588 and 1525 meV. We did not observe any significant changes of the radiative lifetime values with variation of the excitation wavelength. Within the linear excitation regime, we were unable to detect any dependency of the radiative lifetime on the excitation power density within all three of the samples. The fits to the data are obtained by means of a linear regression method using a single exponential decay model. All correlation coefficients (> 0.993) indicate almost flawless fits to the model, thereby ruling out the possibility of other recombination mechanisms, including nonradiative recombination [32]. The inset of Fig. 4 shows the cumulative histogram for the 23% Al sample for all excitation energies, normalized over the entire distribution. The average measured lifetimes for the 13%, 23% and 33% Al samples are (0.87 ± 0.15) ns, (0.93 ± 0.15) ns and (1 ± 0.2) ns, respectively. All computations use the same bin width of 50 ps.

4. Discussion

The measured radiative lifetime values of Fig. 4a agree well with previously reported values of InAs quantum dots in GaAs [12, 33, 34, 35]. On average, the measured radiative lifetimes show no clear observable dependence on either the aluminum concentration or on the exciton transition energy. Based on the values for the radiative lifetime, the transform-limited optical linewidth yields a value close to 1 μeV [19]. Thus we conclude that the measured linewidths of Fig. 2, which are 100$\times$ larger, are not determined by the radiative recombination rate.

We propose that the observed behavior of the linewidth as function of aluminum composition and for both the proper and pre-dots, displayed in Figs. 2 and 3, respectively, is due to spectral wandering, caused by charging and de-charging of local defects in the $Al_xGa_{(1-x)}As$ layer. We expect the density of defects to become larger with increasing aluminum content [27]. This explains the results in Fig. 2, which show that the linewidth of the dots increases when the aluminum concentration rises above a critical value of about 30%. The results of Fig. 3 show that the pre-dots are more sensitive to the charge fluctuations in comparison to the proper dots. This is explained by a weaker localization of the exciton wave function. For decreasing localization, i.e., with decreasing confinement energy, we expect the electron and hole wave functions $\Psi(\mathbf{r}, t)$ to increasingly leak into the surrounding $Al_xGa_{(1-x)}As$ barrier. As a result, the transition becomes more susceptible to the QCSE caused by an induced electric field. This dynamical electric field can be accounted for by assuming charge trapping and detrapping in the vicinity of the dot [17, 36, 37].

If we again turn our attention to the results of Fig. 4, we notice a large variation of the radiative lifetime at a given photon energy (light gray dots). In our case, the deviation of τ_X for the selected dots is 0.61–1.37 ns, which is more than a factor of two. This behavior is different from what has been reported for the InAs quantum dots in GaAs, where the variation is less than 70% [35].

The quantum dot radii ($\approx$12 nm) are smaller than the Bohr radius a_B [33] of approximately 20 nm. Therefore, we conclude that our dots are in the regime of strong confinement [39, 40, 41]. In this regime of strong confinement, the radiative lifetime τ_X is inversely proportional to the overlap between the

electron and hole wave functions [42, 35, 43, 44], i.e., $|\langle\Psi_e|\Psi_h\rangle|^2$. The shortest radiative lifetime corresponds to a maximum overlap of the electron and hole wave functions. The presence of additional defects in the AlGaAs matrix explains the weakening (strengthening) of the oscillator strength of the electron hole pair, owing to a built-in electric field that decreases (increases) the overlap of the electron and hole wave functions via the QCSE.

We calculate the radiative lifetime and emission energy dependence on an applied electric field of an InAs quantum dot embedded in an $Al_{0.23}Ga_{0.77}$ matrix, using a eight band $\mathbf{k}\cdot\mathbf{p}$ model [38] (see Fig. 5). The figure demonstrates how an applied electric field perpendicular to the growth direction reduces the overlap between the electron and hole wave functions through the d.c. Stark effect, confirmed by the redshift of the emission energy. This reduced overlap ultimately leads to a prolongation of the radiative lifetime. Conversely, an electric field applied parallel to the growth direction imposes a negligible effect on both the radiative lifetime and emission energy, validating the strong confinement regime of our dots.

The calculations also demonstrate that the spread in the radiative lifetimes for our dots can be explained by an in-plane electric field of about 50–60 kV/cm. Therefore, we suspect a possible hideout for the charge traps at the alloy fluctuations between the InAs wetting layer and $Al_xGa_{(1-x)}As$ interface. This seems to be the most straightforward and reasonable explanation for the variation in radiative lifetime.

We have performed temperature dependent measurements of the radiative lifetime on several individual quantum dots to exclude phonon assisted carrier escape for the enhancement in the radiative emission rate [21, 45]. These measurements indicate that the radiative lifetime remains constant for temperatures below 35 K, thereby ruling out phonon assisted carrier escape as a possible mechanism.

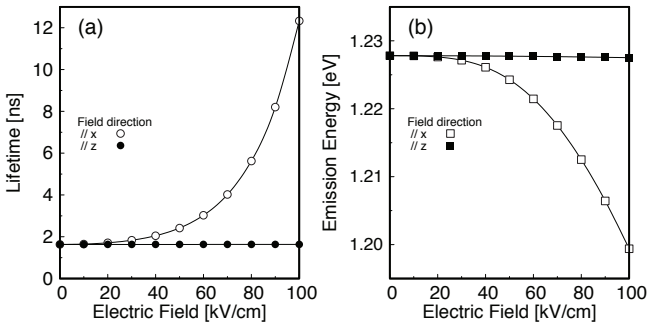

Figure 5. $\mathbf{k}\cdot\mathbf{p}$ calculations demonstrating the influence of an applied electric field on the radiative lifetime (a) and emission energy (b). Calculations were conducted for a quantum dot with a height of 2 nm and a radius of 10 nm. The dot is embedded in an $Al_{0.23}Ga_{0.77}As$ matrix, assuming a non-negligible intermixing of Ga into the InAs quantum dot of 25%. Electric field is applied both perpendicular (open symbols) and parallel (solid symbols) to the growth direction, taking into account the Coulomb interaction of the electron hole pair. For details on the used material parameters and a short explanation of the model theory, see Ref. [38].

5. Conclusions

In summary, we discuss the linewidth broadening of individual quantum dots as function of photon energy. This we consider to be the result of local charging and de-charging of charge centers in the vicinity of the dot, caused by randomized defect incorporation into the $Al_xGa_{(1-x)}As$ matrix. The density of charge traps increases with increasing aluminum content, constituting a local built-in electric field. This electric field leads to larger broadening of individual exciton transitions through the QCSE. For dots that have a high photon energy, i.e., the pre-dots, the decreased localization of the exciton wave function leads to an enhancement of the linewidth broadening. For the first time, we have performed time-resolved measurements on individual InAs quantum dots within a strong confining $Al_xGa_{(1-x)}As$ barrier matrix. Our time correlated measurements reveal that small variations of the electrostatic potential in the local environment of the dot are non-negligible and have a profound effect on the radiative lifetime of the dot.

Acknowledgments

A. A. T., G. V. K. and S. V. I. acknowledge financial support of MBE technology by the Russian Science Foundation, RSF (Project no. 14–22–00107). P. M. K. and A. Yu. S. also acknowledge the financial support of the RSF (Project no. 14–42–00015) during their visit to the Ioffe Institute, when the idea behind the experiments was conceived and the samples were initially characterized. Nanofabrication of the samples was carried out by S. C. M. G. in the Nanolab@TU/e cleanroom facility.

References

[1] Esaki L and Tsu R 1970 *IBM J. Res. Dev.* **14** 61–& ISSN 0018-8646

[2] Solomon P M and Morkoc H 1984 *IEEE Trans. Electron Dev.* **31** 1015–1027 ISSN 0018-9383

[3] Simons R N 1987 *IEEE T. Microw. Theory* **35** 1444–1455 ISSN 0018-9480

[4] Alferov Z I, Vasilev A M, Ivanov S V, Kop'ev P S, Ledentsov N N, Lutsenko M E, Meltser B Y and Ustinov V M 1988 *Pisma Zh. Tekh. Fiz+* **14** 1803–1807 ISSN 0320-0116

[5] Ustinov V M, Egorov A Y, Kovsh A R, Zhukov A E, Maximov M V, Tsatsulnikov A F, Gordeev N Y, Zaitsev S V, Shernyakov Y M, Bert N A, Kop'ev P S, Alferov Z I, Ledentsov N N, Bohrer J, Bimberg D, Kosogov A O, Werner P and Gosele U 1997 *J. Crys. Growth* **175**

689–695 ISSN 0022-0248 9th International Conference on Molecular Beam Epitaxy (MBE-IX), Pepperdine Univ., Malibu, CA, Aug. 05-09, 1996
[6] Maximov M, Shernyakov Y M, Tsatsulnikov A F, Lunev A V, Sakharov A V, Ustinov V M, Egorov A Y, Zhukov A E, Kovsh A R, Kop'ev P S, Asryan L V, Alferov Z I, Ledentsov N N, Bimberg D, Kosogov A O and Werner P 1998 *J. Appl. Phys.* **83** 5561–5563 ISSN 0021-8979
[7] Grinberg A A, Shur M S, Fischer R J and Morkoc H 1984 *IEEE Trans. Electron Dev.* **31** 1758–1765 ISSN 0018-9383
[8] Levine B F 1993 *J. Appl. Phys.* **74** R1–R81 ISSN 0021-8979
[9] Mailly D, Chapelier C and Benoit A 1993 *Phys. Rev. Lett.* **70** 2020–2023 ISSN 0031-9007
[10] Noborisaka J, Motohisa J, Hara S and Fukui T 2005 *Appl. Phys. Lett.* **87** ISSN 0003-6951
[11] Tomioka K, Motohisa J, Hara S, Hiruma K and Fukui T 2010 *Nano Lett.* **10** 1639–1644 ISSN 1530-6984
[12] Borri P, Langbein W, Schneider S, Woggon U, Sellin R L, Ouyang D and Bimberg D 2001 *Phys. Rev. Lett.* **87** ISSN 0031-9007
[13] Birkedal D, Leosson K and Hvam J M 2001 *Phys. Rev. Lett.* **87** 227401 ISSN 0031-9007
[14] Kroner M, Remi S, Högele A, Seidl S, Holleitner A W, Warburton R J, Gerardot B D, Petroff P M and Karrai K 2008 *Physica E* **40** 1994–1996 ISSN 1386-9477 13th International Conference on Modulated Semiconductor Structures (MSS13)/17th International Conference on Electronic Properties of 2-Dimensional Systems, Genova, Italy, Jul. 15-20, 2007
[15] Warburton R J, Schulhauser C, Haft D, Schäflein C, Karrai K, Garcia J M, Schoenfeld W and Petroff P M 2002 *Phys. Rev. B* **65** ISSN 1098-0121
[16] Gammon, D and Snow, E S and Shanabrook, B V and Katzer, D S and Park, D 1996 *Science* **273** 87–90 ISSN 0036-8075
[17] Houel J, Kuhlmann A V, Greuter L, Xue F, Poggio M, Gerardot B D, Dalgarno P A, Badolato A, Petroff P M, Ludwig A, Reuter D, Wieck A D and Warburton R J 2012 *Phys. Rev. Lett.* **108** ISSN 0031-9007
[18] Bayer M and Forchel A 2002 *Phys. Rev. B* **65** ISSN 1098-0121
[19] Kuhlmann A V, Houel J, Ludwig A, Greuter L, Reuter D, Wieck A D, Poggio M and Warburton R J 2013 *Nat. Phys.* **9** 570–575 ISSN 1745-2473
[20] Jagdeep Shah 1996 *Ultrafast spectroscopy of semiconductors and semiconductor nanostructures* (Berlin: Springer) ISBN 3-540-60912-1
[21] Besombes L, Kheng K, Marsal L and Mariette H 2001 *Phys. Rev. B* **63** ISSN 0163-1829
[22] Favero I, Cassabois G, Ferreira R, Darson D, Voisin C, Tignon J, Delalande C, Bastard G, Roussignol P and Gérard J M 2003 *Phys. Rev. B* **68** ISSN 1098-0121
[23] Klauder J R and Anderson P W 1962 *Phys. Rev.* **125** 912–& ISSN 0031-899X
[24] Bhattacharyya D, Avrutin E A, Bryce A C, Marsh J H, Bimberg D, Heinrichsdorff F, Ustinov V M, Zaitsev S V, Ledentsov N N, Kop'ev P S, Alferov Z I, Onischenko A I and O'Reilly E P 1999 *IEEE J. Sel. Top. Quant.* **5** 648–657 ISSN 1077-260X
[25] Vurgaftman I, Meyer J R and Ram-Mohan L R 2001 *J. Appl. Phys.* **89** 5815–5875 ISSN 0021-8979
[26] Pavesi L and Guzzi M 1994 *J. Appl. Phys.* **75** 4779–4842 ISSN 0021-8979
[27] Offermans P, Koenraad P M, Wolter J H, Pierz K, Roy M and Maksym P A 2005 *Phys. Rev. B* **72** ISSN 1098-0121
[28] Aspnes D E, Kelso S M, Logan R A and Bhat R 1986 *J. Appl. Phys.* **60** 754–767 ISSN 0021-8979
[29] Brunner K, Abstreiter G, Bohm G, Trankle G and Weimann G 1994 *Appl. Phys. Lett.* **73** 1138–1141 ISSN 0031-9007
[30] Sallen G, Tribu A, Aichele T, Andre R, Besombes L, Bougerol C, Richard M, Tatarenko S, Kheng K and J-Ph Poizat 2010 *Nat. Photonics* **4** 696–699 ISSN 1749-4885
[31] Monniello L, Reigue A, Hostein R, Lemaitre A, Martinez A, Grousson R and Voliotis V 2014 *Phys. Rev. B* **90** ISSN 1098-0121
[32] Yu H P, Lycett S, Roberts C and Murray R 1996 *Appl. Phys. Lett.* **69** 4087–4089 ISSN 0003-6951
[33] Hours J, Senellart P, Peter E, Cavanna A and Bloch J 2005 *Phys. Rev. B* **71** ISSN 1098-0121
[34] Campbell-Ricketts T E J, Kleemans N A J M, Nötzel R, Silov A Y and Koenraad P M 2010 *Appl. Phys. Lett.* **96** ISSN 0003-6951
[35] Dalgarno P A, Smith J M, McFarlane J, Gerardot B D, Karrai K, Badolato A, Petroff P M and Warburton R J 2008 *Phys. Rev. B* **77** ISSN 1098-0121
[36] Kamada H and Kutsuwa T 2008 *Phys. Rev. B* **78** ISSN 1098-0121
[37] Vogel M M, Ulrich S M, Hafenbrak R, Michler P, Wang L, Rastelli A and Schmidt O G 2007 *Appl. Phys. Lett.* **91** ISSN 0003-6951
[38] Pryor C 1998 *Phys. Rev. B* **57** 7190–7195 ISSN 1098-0121
[39] Takagahara T 1987 *Phys. Rev. B* **36** 9293–9296 ISSN 1098-0121
[40] Andreani L C, Panzarini G and Gérard J M 1999 *Phys. Rev. B* **60**(19) 13276–13279 ISSN 1098-0121
[41] Bellessa J, Voliotis V, Grousson R, Wang X L, Ogura M and Matsuhata H 1998 *Phys. Rev. B* **58** 9933–9940 ISSN 1098-0121
[42] Sugawara M 1995 *Phys. Rev. B* **51** 10743–10754 ISSN 0163-1829
[43] Stobbe S, Kristensen P T, Mortensen J E, Hvam J M, Mork J and Lodahl P 2012 *Phys. Rev. B* **86** ISSN 1098-0121
[44] Dawson P, Ma Z, Pierz K and Gobel E O 2002 *Appl. Phys. Lett.* **81** 2349–2351 ISSN 0003-6951
[45] Takagahara T 1999 *Phys. Rev. B* **60** 2638–2652 ISSN 1098-0121